Influential factors on the performance of embankments stabilised on deep-mixed columns

Downloaded from: https://research.chalmers.se, 2025-09-25 23:02 UTC

Citation for the original published paper (version of record):
Bozkurt, S., Dijkstra, J., Karstunen, M. (2025). Influential factors on the performance of embankments stabilised on deep-mixed columns. Transportation Geotechnics, 55. http://dx.doi.org/10.1016/j.trgeo.2025.101643

N.B. When citing this work, cite the original published paper.

research.chalmers.se offers the possibility of retrieving research publications produced at Chalmers University of Technology. It covers all kind of research output: articles, dissertations, conference papers, reports etc. since 2004. research.chalmers.se is administrated and maintained by Chalmers Library

(article starts on next page)

Transportation Geotechnics 55 (2025) 101643

Contents lists available at ScienceDirect

Transportation Geotechnics

journal homepage: www.elsevier.com/locate/trgeo

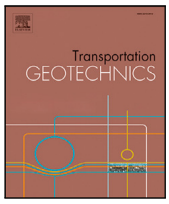

Original article

Influential factors on the performance of embankments stabilised on deep-mixed columns

Sinem Bozkurt *, Jelke Dijkstra, Minna Karstunen

Chalmers University of Technology, Department of Architecture and Civil Engineering, Gothenburg, SE-412 96, Sweden

ARTICLE INFO

Keywords:
Experimental design
Volume averaging
Deep mixing
Sensitivity analysis
Soft clay

ABSTRACT

The realistic estimation of the hydromechanical response of embankments on soft clay, stabilised with lime-cement columns, relies heavily on the accurate modelling of both *in situ* clay and the columns of the three-dimensional (3D) problem. This study simulates the 3D effects using a homogenisation technique, while the quantification of the most influential parameters governing the stress–strain response of the stabilised clay is assessed through the Design of Experiments (DOE). The governing mechanisms in relation to the full range of model parameters for various stabilisation ratios and length configurations, including end-bearing and floating columns, are investigated. Subsequently, to reduce the costs originating from the use of lime and cement and the associated anthropogenic greenhouse gas emissions, the key relationship between column length, stabilisation ratio and relative stiffness between the clay and columns is explored. The proposed systematic approach enables efficient incorporation of sensitivity studies and reduces computational demand in the design phase, enabling optimisation.

1. Introduction

Ground improvement using columnar inclusions, such as stone columns and lime-cement (LC) columns, is commonly used for improving the properties of soft natural clays, especially in urban areas where the design is controlled by displacements. In the dry deep mixing method (DSM), common in the Nordic countries, the typical admixtures used include Ordinary Portland cement (OPC) [1] and unslaked lime (QL). In DSM the natural soft clay, cement and lime in dry powder form are mixed *in situ* to create columns, called lime-cement (LC) columns [2,3]. LC columns improve the stability of embankments and reduce total and differential settlements, thereby lowering future maintenance costs. Due to the large amounts of material and energy used in the construction of LC columns [4], however, DSM contributes significantly to anthropogenic greenhouse gas emissions, due to the manufacturing processes of lime [5,6] and cement [7–9].

To integrate the environmental impacts in the assessment of the final performance of the ground improvement system, life-cycle analysis (LCA) of the products over their lifetime [e.g. 10–13] together with a streamlined energy and emissions assessment model (SEEAM) for quantifying energy consumption and $C0_2$ emissions [i.e. 14–16] emerge as assisting tools. However, existing transport infrastructure is often associated with high maintenance expenses [17,18]. For example, in Sweden about 46% of the total budget for the transport infrastructure is allocated to maintaining existing roads and railways, which is expected to increase in the coming years [19].

One of the main drivers for the high (often reactive) maintenance costs is associated to nonuniform alignment caused by differential settlements of linear transport infrastructure in areas with soft soils. Maintenance costs can be significantly reduced during the design phase by optimisation. This requires numerical analyses that accurately capture the hydromechanical response of natural clays, including features such as anisotropy, stress history, and hardening/ softening. The time-dependent deformations in the natural soft clays beneath the railway and road embankments can then be estimated with adequate precision [e.g. 20–23]. In addition, the response of the stabilised clay in the columns needs to be realistically incorporated. Costs can be further minimised by reducing uncertainties at the site through sufficient geotechnical site investigation, and determination of the soil properties (hence model parameters) that matter the most. Identification of the most influential parameters combined with high-fidelity predictive models is an essential first step to minimise risks, optimise performance, and reduce environmental impact, and paves the way to developing methods for predictive maintenance and performance-based design [24–27].

Advanced numerical simulations are required to account for the different constitutive behaviour of *in situ* clay and the columns, in order

* Corresponding author.
E-mail address: sinem.bozkurt@chalmers.se (S. Bozkurt).

https://doi.org/10.1016/j.trgeo.2025.101643
Received 23 May 2025; Received in revised form 10 June 2025; Accepted 8 July 2025
Available online 26 July 2025
2214-3912/© 2025 The Authors. Published by Elsevier Ltd. This is an open access article under the CC BY license (http://creativecommons.org/licenses/by/4.0/).

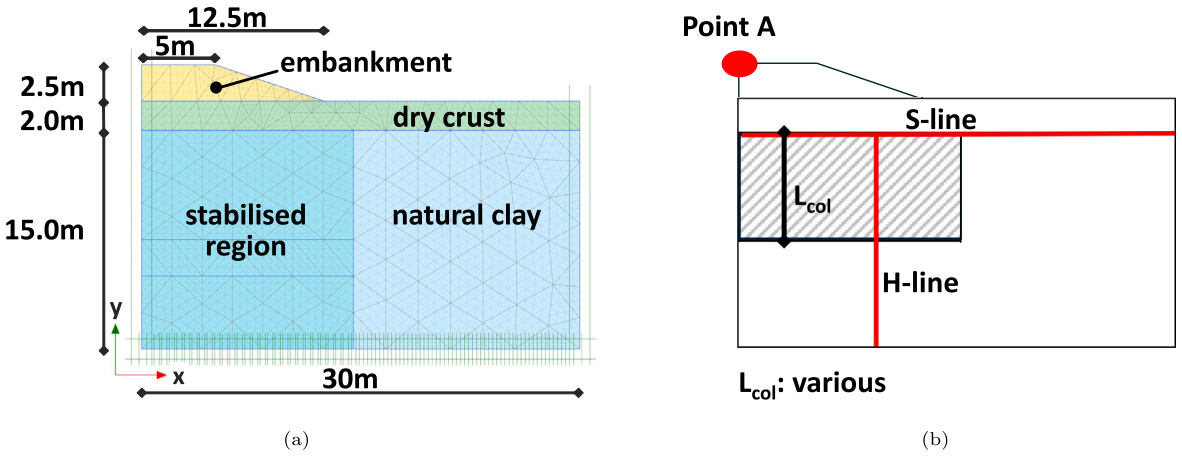

Fig. 1. Geometry of embankment: (a) discretised geometry; (b) displacement readings.

to accurately predict the settlements and horizontal movements due to the construction of embankments on soft clay deposits stabilised with deep-mixed columns. Volume averaging technique (VAT) is a well-established advanced numerical method that can realistically represent the hydromechanical response of stabilised soft clays [i.e. 28–32]. The technique accounts for the response of the individual materials (i.e. soft clay and deep-mixed columns) and enables to map the inherently 3D problem to an equivalent two-dimensional (2D) counterpart. The fundamental feature of the technique is its ability to represent the composite material, consisting of natural clay and deep-mixed columns, with an equivalent homogenised material, while still enabling to track the stress–strain response of the individual components. VAT is a powerful technique that enables the system level modelling of the 3D composite in 2D plane strain analyses, ensuring the strain compatibility of the materials involved. The originality of the paper is to take advantage of the computational efficiency of VAT for a global sensitivity study using the Design of Experiments (DOE) approach [33], whilst maintaining high fidelity and the ability to study the interaction between column materials and the surrounding soil.

This study aims to identify the most influential parameters governing the settlements of an embankment stabilised with LC columns for Serviceability Limit State (SLS). In this paper, by employing advanced constitutive models for individual materials (soft clay and LC columns) through VAT, a series of sensitivity analyses are performed using the finite element (FE) method. The method of DOE is first employed in these 2D plane strain analyses with VAT to systematically examine the effects of geotechnical model parameters and their interactions on the response of the system. The systematic approach adopted provides a comprehensive understanding of the factors influencing the fully coupled hydromechanical response of stabilised embankments.

The evolution of deformations with time are investigated in relation to various stabilisation ratios (different column spacings), column length configurations (end-bearing and floating), and the full range of model parameters, including those of the S-CLAY1S [34] and MN-hard [35] models for soft clay and LC columns, respectively. The combination of VAT and DOE enhances computational efficiency and ensures the identification of influential model parameters, including column material and surrounding soil. This in turn enables the optimisation of deep-mixing designs to minimise material consumption (lime and cement) and their associated climate impact.

2. Numerical framework

2.1. Numerical model of an embankment

Numerical analyses were performed assuming a typical case, a 2.5 m high embankment with a top width of 10 m and a base width of 25 m, and side slopes inclined at 3H:1V. The soil stratigraphy consists of a 2 m thick layer of dry crust overlying a deep soft clay deposit. The long-term deformations were simulated by accounting for the transient flow, and snapshots of the results were taken at three specific locations: the top of the embankment (Point A), the longitudinal axis at the top of the soft clay deposit (S-line), and along the vertical plane within the soft clay deposit (H-line) (see Fig. 1(b)). The groundwater level was assumed to be at the boundary between the dry crust and the soft clay layers, at a depth of 2 m. For the reference cases, LC columns with a diameter of 0.7 m were assumed to be arranged in a square grid with 1 m centre to centre spacing. Maintaining high quality in the columns near the surface of the soil, in the desiccated ('dry') crust, is challenging [36], therefore it was assumed that the columns extended only through the soft clay deposit with varying lengths of 7.5 m, 10 m, and 15 m.

In the analysis, the construction of the LC column in the stabilised region was assumed to be wished-in-place, and therefore the installation effects during and after the deep mixing process were not accounted for. These effects can be integrated into the simulation through external strain or load applications, provided that relevant field instrumentation data are available [i.e. 28,37].

The embankment geometry is shown in Fig. 1(a) for a case with end-bearing columns with a length of 15 m. To minimise the discretisation effects, the same geometry is utilised in the simulations of different scenarios, such as the cases without soil improvement and the cases with various LC column lengths. The final mesh comprises 235 15-noded triangular elements, totalling 1987 nodes. Exploiting the symmetry, only half of the embankment is simulated. The standard fixities are applied as the displacement boundary conditions. The hydraulic boundaries at both the symmetry axis and the bottom are modelled as impermeable, with the latter due to the consideration of the deep soft clay deposit resting on an impermeable bedrock.

In this study, the S-CLAY1S model [34,38] is used to simulate the behaviour of the natural clay, by accounting for the initial anisotropy, the evolution of fabric and the strain-softening. When modelling embankments stabilised with deep-mixed columns for SLS, priority is given to stress-dependent stiffness and the influence of soft clay on the overall response, rather than to the yielding and post-peak response of the columns. The so-called MNhard model [35] is employed to capture the non-linear behaviour of the columns. The model uses the hyperbolic stress–strain relationship for shear hardening, and the ultimate failure is computed based on the Matsuoka–Nakai failure criterion that is the average of the spatially mobilised planes (SPM) in 3D effective stress space [39,40]. The formulations of the models are presented in Appendices B and C.

The model parameters for the natural clay and the LC columns are selected based on prior study by [37], aiming to ensure the application of realistic model parameters for the numerical analysis of a stabilised

Table 1
Parameter ranges for soft natural clay.

Parameter	Definition	Unit	Lower boundary	Mean values	Upper boundary
κ	Slope of the swelling line	[-]	0.0195	0.02	0.0205
ν'_{clay}	Effective Poisson's ratio of clay	[-]	0.195	0.20	0.205
λ_i	Slope of the intrinsic normal compression line	[-]	0.195	0.20	0.205
M	Critical state stress ratio	[-]	1.073	1.10	1.128
ω	Absolute effectiveness of rotational hardening	[-]	48.75	50	51.25
ω_d	Relative effectiveness of rotational hardening	[-]	0.624	0.64	0.656
ξ	Absolute rate of destructuration due to volumetric strain	[-]	11.7	12.0	12.3
ξ_d	Relative rate of destructuration due to shear strain	[-]	0.39	0.40	0.41
POP	preoverburden pressure	[kPa]	19.5	20.0	20.5
α_0	Initial anisotropy	[-]	0.410	0.42	0.431
χ_0	Initial amount of bonding	[-]	5.85	6.0	6.15

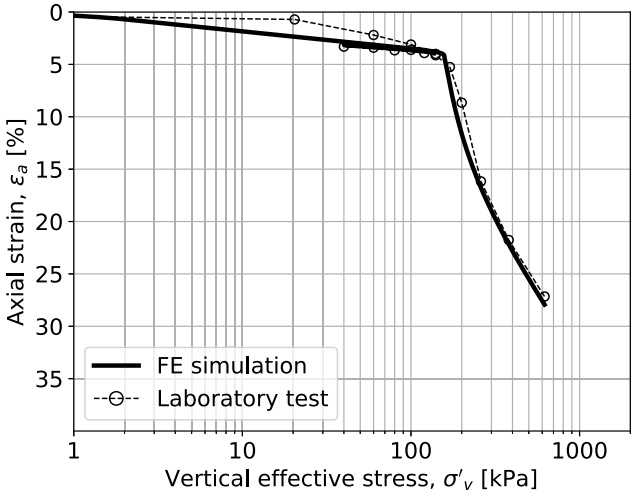

Fig. 2. Calibration of model parameters for the soft clay layer using data from the oedometer test.

embankment on soft clay. As described in [37], data from a series of anisotropically consolidated triaxial tests and incrementally loaded oedometer tests performed on natural soft clay and LC column samples were used. The procedures outlined by [41,42] were followed: standard parameters were first derived from fall cone, oedometer, and triaxial tests, while non-standard parameters were selected within the ranges proposed by [42] and subsequently calibrated at single integration point using simulations of the element level tests via the SoilTest facility in the PLAXIS 2D FE code, as illustrated in Fig. 2.

The model parameters for the soft clay and LC column materials are presented in Tables 1 and 2, respectively. The vertical and horizontal hydraulic conductivities of the soil are assumed to be equal ($k_v = k_h$), approximately 0.75×10^{-4} m/day. The dry crust was simulated using the Hardening Soil model [43], while the Mohr Coulomb model was chosen to simulate the embankment fill (refer to Tables D.8 and D.9 in Appendix D).

2.2. Homogenisation technique

LC columns are constructed under embankments in a variety of 3D periodic forms, such as single columns, panels, grids, or blocks [44–46], which in principle require models that account for the distinct stress–strain responses of the soft natural clay and the stabilised clay (i.e. LC columns), as well as the 3D geometrical effects.

Often, analytical and simplified numerical methods have aimed to simplify the 3D problem to an equivalent plane strain model, utilising an average stiffness based on the area replacement ratio of the stabilised region [27,37,47–51]. This approach is reasonable if both materials behave in an elastic manner, with a stiffness that is independent of the effective stress and loading history that is not the case. Furthermore, in numerical analyses with elasto-plastic models, the simple stiffness modification methods are an oversimplification. Therefore, the numerical methods adopted herein are expected to capture the coupled hydromechanical response of the stabilised clay as well as the *in situ* soft clay for SLS [52]. Moreover, even though the embankment construction is often considered as a one-dimensional loading problem, shearing and the rotation of principal stresses need to be taken into account for realistic estimates of both vertical and lateral deformations [20,34,53].

To overcome these limitations, a rigorous homogenisation technique has been proposed for calculating the settlements of embankments underlain by soft clay deposits [28–30,32] stabilised with columnar inclusions (LC columns or stone columns). The technique employs different constitutive models for describing the elasto-plastic responses of the *in situ* clay and the column material. The composite material, made of natural clay and columns, is replaced with an equivalent homogenised material. The interaction effects between individual materials are based on the local equilibrium and kinematic constraints proposed by [29] and have been derived to construct a 2D VAT formulation. These constraints were subsequently verified in [30] by comparing 2D and 3D simulations, and validated against field cases by [32]. The stress–strain response of the equivalent material can then be calculated by averaging the constitutive behaviour of the individual materials based on their respective volume fractions. The fundamental assumption is the averaging rule in Eq. (1).

$$(\boldsymbol{\Delta\sigma}^{\mathbf{eq}})' = \Omega_s(\boldsymbol{\Delta\sigma}^{\mathbf{s}})' + \Omega_{col}(\boldsymbol{\Delta\sigma}^{\mathbf{col}})' \tag{1}$$

$$\boldsymbol{\Delta\varepsilon}^{\mathbf{eq}} = \Omega_s\boldsymbol{\Delta\varepsilon}^{\mathbf{s}} + \Omega_{col}\boldsymbol{\Delta\varepsilon}^{\mathbf{col}} \tag{2}$$

where $(\boldsymbol{\Delta\sigma}^{\mathbf{eq}})'$ and $\boldsymbol{\Delta\varepsilon}^{\mathbf{eq}}$ stand for the increments of the effective stress and strain tensors of the equivalent material, respectively. The subscripts *col* and *s* denote columns and soft clay. Ω is the volume fraction that can be computed considering the representative area of the constituents, dependent on how the columns are distributed.

The computation uses the elastic stiffness matrices of individual materials to compute the stiffness matrix of the equivalent material, $\mathbf{D}^{\mathbf{eq}}$ according to Eq. (3).

$$\mathbf{D}^{\mathbf{eq}} = \Omega_s\mathbf{D}^{\mathbf{s}}\mathbf{S}^{\mathbf{s}} + \Omega_{col}\mathbf{D}^{\mathbf{col}}\mathbf{S}^{\mathbf{col}} \tag{3}$$

Eq. (3) is based on the assumption that the local equilibrium and kinematics of the strain field will be maintained, specifically that the constitutive constraints are ensured by strain decomposition matrices $\mathbf{S}^{\mathbf{s,col}}$ using the following assumptions. The global coordinate system in a 2D analysis defines x and z as horizontal directions and y as vertical. Local mechanical balance can be described as:

$$\Delta\sigma_{xx}^{eq} = \Delta\sigma_{xx}^{col} = \Delta\sigma_{xx}^{s} \tag{4}$$

Table 2
Parameter ranges for LC columns.

Parameter	Definition	Unit	Lower boundary	Mean values	Upper boundary
G_{50}	Secant shear stiffness	[kPa]	27 300	28 000	28 700
G_{ur}	Un-/re-loading shear stiffness	[kPa]	73 125	75 000	76 875
c'_{col}	Effective cohesion	[kPa]	19.5	20.0	20.5
ϕ'_{col}	Effective friction angle	[°]	36.1	37.0	37.9
Ω_{col}	Fraction of columns	[-]	0.37	0.38	0.39
ν'_{col}	Effective Poisson's ratio of columns	[-]	0.244	0.25	0.256
f_{tens}	Allowable tensile stress	[kPa]	9.75	10.0	10.25

$$\Delta\sigma_{zz}^{eq} = \Delta\sigma_{zz}^{col} = \Delta\sigma_{zz}^{s} \quad (5)$$

$$\Delta\tau_{xy}^{eq} = \Delta\tau_{xy}^{col} = \Delta\tau_{xy}^{s} \quad (6)$$

$$\Delta\tau_{yz}^{eq} = \Delta\tau_{yz}^{col} = \Delta\tau_{yz}^{s} \quad (7)$$

Kinematic constraints for the case of a stabilised clay can be imposed as:

$$\Delta\varepsilon_{yy}^{eq} = \Delta\varepsilon_{yy}^{col} = \Delta\varepsilon_{yy}^{s} \quad (8)$$

$$\Delta\gamma_{zx}^{eq} = \Delta\gamma_{zx}^{col} = \Delta\gamma_{zx}^{s} \quad (9)$$

The local integration utilises an implicit scheme to iteratively solve the system of nonlinear equations. Using $\mathbf{D}^{eq}$, the equivalent strain increment, $\boldsymbol{\Delta\varepsilon}^{eq}$ is estimated at the stress integration points using the standard FE procedure. During iterations, if equilibrium is not met, the stress states revert to their previous values, and the strain increments are re-apportioned among the constituents using standard return mapping schemes [54].

The homogenisation procedure is implemented with an in-house User Defined Model (UDSM) for the commercial FE code PLAXIS 2D (version 2024), based on [55]. This study adopts the current implementation of VAT by [32,55] that accounts for the stress–strain responses of the natural clay and the LC columns using the S-CLAY1S [34,38] and MNhard [35] models.

3. Global sensitivity analysis

Global sensitivity analysis (GSA) explores how individual factors or groups of factors contribute to the uncertainty in the model output. In contrast to the One-Variable-At-a-Time (OVAT) approach, this systematic approach can statistically assess the interactions between factors. However, in geotechnics, GSA has seldom been employed due to the traditional reliance on OVAT in parametric studies of stabilised embankments [e.g. 56–58]. OVAT investigates the uncertainty of the output by varying one factor at a time, while keeping all others fixed between sequential simulations, based largely on intuition. When the problem is complex, due to a large number of factors affecting the system response, OVAT becomes computationally expensive and impractical in quantifying the induced uncertainty [33,59]. Often, there is no guarantee that the effect of a factor will remain the same when there is a change in the level of another factor. Therefore, most of the time, the results of OVAT can be misleading and can thus lead to unsatisfactory conclusions in real-life situations [60,61]. In contrast, a systematic approach employing for example the Design of Experiments (DOE) becomes essential to identify the key factors in models with many factors [62].

3.1. Design of experiments (DOE)

DOE is a powerful tool for assessing the influence of several variables on a certain characteristic of the design output by factorial designs [33,63,64]. DOE involves investigating all possible combinations of factors using a full factorial design or examining the main effects (i.e. primary factors) and low-order interactions using a fractional factorial design. Fractional factorials are usually employed as screening designs in the initial stage. Each factor is studied at two levels, but only a fraction of all factor-level combinations is analysed, thereby reducing a relatively large list of factors to a manageable number.

The primary objective in screening experiments is to identify significant factors in the predicted response, while fitting an empirical response surface model is relatively unimportant at this stage. In geotechnical engineering, the DOE method has been employed to realistically quantify the induced uncertainty in the mixing process. Several factors (i.e. retrieval rate, number of mixing blades, rotational speed, air pressure) were investigated using two- and 2^k factorial experiments [65,66]. Later, [67] utilised DOE to assess the spatial correlation structure on the variability of LC columns in the horizontal direction using penetrometer test data, as a measure of mixing quality. The method is also adopted in the calibration process for soil model parameters, highlighting the non-stationary nature of factor screening for time-dependent processes [68].

In this study, DOE was used to evaluate the most influential parameters of the soil models that affect the long-term hydromechanical response of an embankment stabilised with LC columns. The time-dependent settlements and horizontal displacements were computed using finite element analyses (FEA) (PLAXIS 2D, version 24). The design methodology is given in Fig. 3. The implementation of the DOE procedure was facilitated using pyDOE2[1] via Python interpreter while performing FEA.

Initially, the factors and their two levels (i.e. the ranges of upper and lower bounds) are identified. Then, depending on full or fractional factorial design considerations, the standard design matrix is constructed for all possible combinations of factor levels. The orthogonality of the design matrix ensures that each estimated effect is not affected by the magnitudes and signs of the other factors. The main effect of a factor is the average difference in response between its high and low levels. An interaction effect occurs when the difference in response between the levels of one factor changes depending on the levels of other factors.

A fractional factorial design is generally represented in the form 2^{k-p}, where k is the number of factors and $1/2^p$ indicates the fraction of the full factorial 2^k [33]. Independent *generators*, p dictate the *defining relation*, which allows the aliasing structure of the design to be easily determined. An aliasing structure may cause the effect of a particular factor or interaction to be indistinguishable from that of another factor or interaction. To overcome any confounding effects, designs with the highest possible *resolution* are desirable so that lower-order effects are not confounded with higher-order effects (third-, fourth-, or higher-order) that are usually assumed to be negligible [33]. As an illustrative example, a table of contrasts and the design generators are presented in Appendix A for a 2^{11-6}_{IV} fractional factorial design, which is of resolution IV. In a resolution IV design, no main effects are confounded with any other main effects or with any two-factor interaction effects, although two-factor interaction effects are confounded with each other.

[1] pyDOE2 is a Python library used for DOE. https://pypi.org/project/pyDOE2/

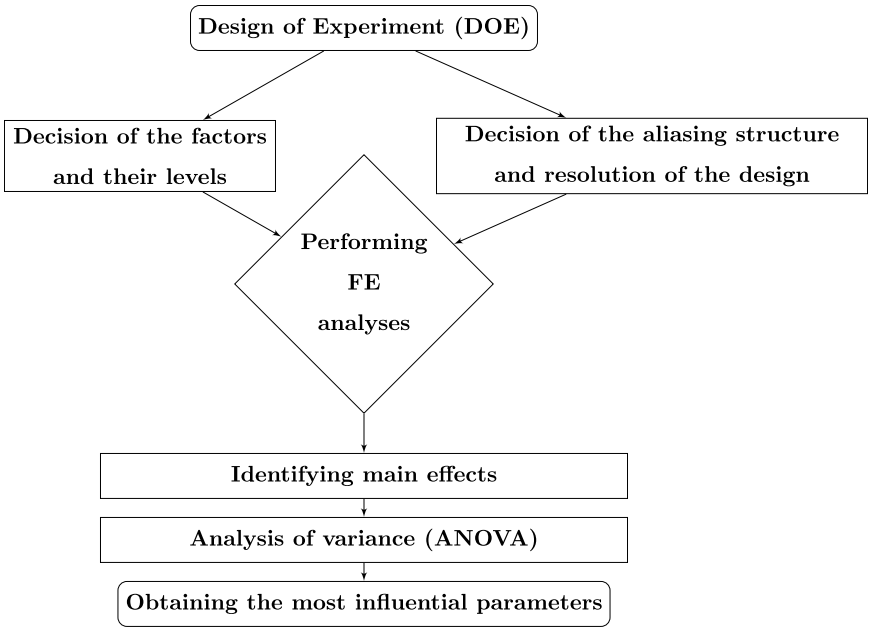

Fig. 3. Flowchart of the Design of Experiments (DOE) methodology.

Table 3
Computed settlements for the average parameter set for different considerations of column length.

	Embankment construction	Consolidation period				
		2 year	10 year	50 year	200 year	500 year
Unimproved	0.043 m	0.086 m	0.198 m	0.482 m	0.825 m	0.927 m
L_{col} = 7.5 m	0.035 m	0.067 m	0.111 m	0.159 m	0.164 m	0.165 m
L_{col} = 10 m	0.034 m	0.062 m	0.089 m	0.100 m	0.100 m	0.100 m
L_{col} = 15 m	0.034 m	0.042 m	0.045 m	0.045 m	0.045 m	0.045 m

After a careful examination of the magnitude and direction of the effects to identify the factors with the greatest influence on the system response, the analysis of variance (ANOVA) is utilised.

3.2. Factorial design of an embankment

The influence of the parameters of the soil models on the long-term deformations of an embankment was investigated by considering unimproved natural clay, as well as the stabilisation with varied column lengths (floating and end-bearing columns) ranging from 7.5 m to 15 m, using a fractional factorial design (resolution IV). The parameters of the soil model used in the simulations of the reference case are detailed in Tables 1 and 2. The parameters for both the natural clay (S-CLAY1S) and the column material (MNhard) were considered as independent factors at two levels, with each factor having a 5% difference between the upper and lower boundaries, centred around the reference values incorporated from a previous study [37]. The range has been chosen arbitrarily as an initial step in identifying the influential factors in the numerical model and is thus not linked with the expected natural variability.

A fully coupled numerical analysis of a hypothetical embankment, introduced in Section 2.1, was performed initially for the unimproved case using the S-CLAY1S soil model with the reference mean values presented in Table 1. A fixed arbitrary long time (500 years) was selected to ensure that the excess pore pressures at the end of the analyses are approximately zero for all cases considered. The order of magnitude of the maximum settlement computed at the top of the embankment following the construction indicates the necessity of ground improvement, as can be seen in Table 3. Therefore, a range of lengths of the LC column was used to simulate the response of the stabilised clay with VAT by incorporating the different constitutive models for the soft clay and LC columns using the S-CLAY1S and MNhard soil models, respectively (see Tables 1 and 2). Among the cases with ground improvement, the similarity in the short-term responses demonstrates the importance of time-dependent consolidation analysis, as the distinction becomes more pronounced following the dissipation of the excess pore pressures. Therefore, sensitivity analyses that only consider the short-term effects are likely to yield misleading results.

4. Results

The following section presents the key parameters of the soil models that influence the stabilisation using LC columns in different scenarios, such as varying column lengths and volume ratios, and compares the cases with or without stabilisation. The effect of the parameters of the constitutive models on the magnitude and direction of displacements (settlements and horizontal displacements) is explored with a focus on the long-term response.

4.1. Influential parameters

Based on the long-term sensitivity analyses, the effects of the factors on the maximum settlements recorded at the top of the embankment (Point A) are presented in Fig. 4 for varying column lengths. Due to the significant difference in the rigidity between the columns and natural clay, the overall response of stabilised embankments is often considered to be governed by the column parameters. Nonetheless, Fig. 4 suggests that the dominance of the columns on the computed maximum settlements is more pronounced for the end-bearing columns

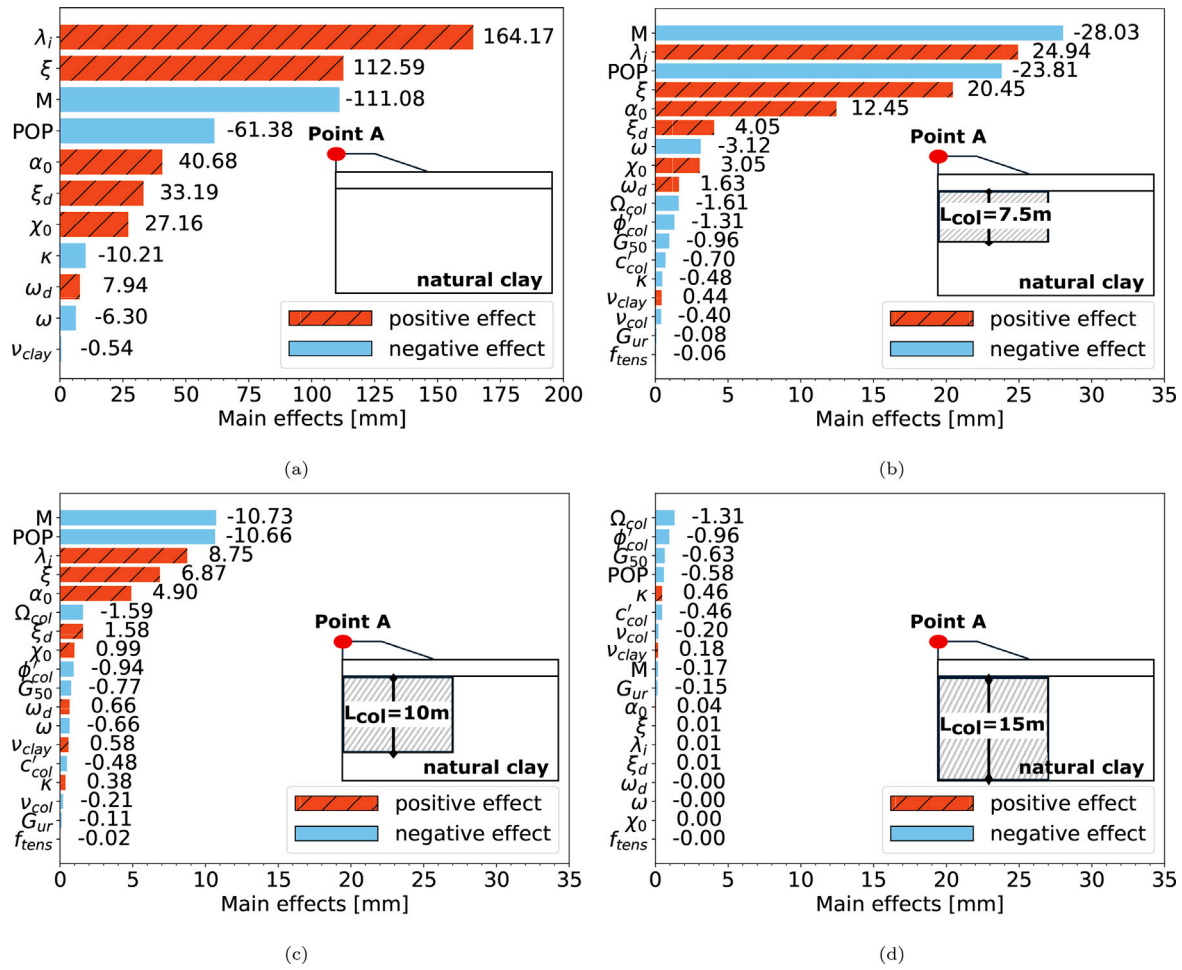

Fig. 4. Main effects plot according to FE simulations using fractional factorial design: (a) natural clay (without stabilisation) 2_{IV}^{11-6}; (b) stabilisation with 7.5 m long columns 2_{IV}^{18-11}; (c) stabilisation with 10 m long columns 2_{IV}^{18-11}; (d) stabilisation with 15 m long columns 2_{IV}^{18-11}.

of 15 m, compared to the floating columns of varying lengths, ranging from 7.5 m to 10 m.

When floating columns (Figs. 4(b) and 4(c)) are used, the parameters that represent the clay response *in situ* have the largest effect on the calculated maximum settlement. An increase in the length of the floating columns resulted in a significant reduction in the magnitude of the settlements, while the order of influence (particularly, for the effects higher than approximately 5 mm) and the direction of the effects remained unchanged. The stress ratio at the critical state (M), preoverburden pressure (POP), intrinsic compression index (λ_i), the state parameter (ξ) describing the initial amount of bonding and the initial anisotropy (α_0) appear to be the most prominent parameters. However, the direction of their effects on the computed settlements varies, resulting in either an increase or a decrease in the predicted settlements. Using the upper bound of the parameters, such as M and POP, led to an expected reduction in the calculated settlements, indicating that the soil has already undergone significant compression under the existing stress conditions. Meanwhile, adopting the upper boundary for λ_i, ξ and α_0 led to increased compressibility and thus resulted in larger irrecoverable straining.

Simulations with 15 m-long end-bearing columns (Fig. 4(d)) result in the least settlements due to the higher stiffness of the system compared to the *in situ* clay. The volume fraction of the columns, Ω_{col} and the reference shear stiffness of the columns, G_{50} have the highest influence on the computed settlements. The model parameter κ for clay, that represents the slope of the swelling line in the compression plane, the shear modulus G_{50} in the columns as well as Ω_{col} are directly linked to the initial stiffness matrix of the homogenised material when VAT is employed. Following the load application, the applied stress is divided between the materials based on their respective fractions and their elastic stiffness matrices. POP holds primary importance in controlling the yield criterion of the S-CLAY1S model. Given the relatively low overburden pressure from the 2.5 m high embankment is comparable to the reference POP, the increased rigidity of the system and the redistribution of the load due to stabilisation with LC columns along the entire compressible depth, there are no large plastic deformations in the natural clay. It should be noted that the strength parameters of the columns (c'_{col} and ϕ'_{col}) are used to calculate the stress-dependent stiffnesses (G_{50} and G_{ur}). Therefore, in Fig. 4(d), the strength of the columns appears to have a significant effect, but as it is only a component of the hyperbolic stress–strain relationship in the formulation of the MNhard model, it is not influential for SLS [69].

The construction of road embankments on soft clay deposits generally results in a substantial rotation of the principal stresses. This is particularly important for lightly overconsolidated soft natural clays with low hydraulic conductivity, which are susceptible to large deformations under shearing. In the case of stabilisation with LC columns, the magnitude of deformations and stress rotations is controlled by the column length, particularly due to the high difference in the rigidity between the columns and natural clay. Larger settlements were calculated for floating columns compared to end-bearing columns, as can be seen in Figs. 5(a) and 5(b), at the top of the embankment (Point A) and along the surface of the soft clay (S-line), respectively.

Similarly, the horizontal displacement profiles underneath the stabilised embankment (H-line) for varying column lengths show that

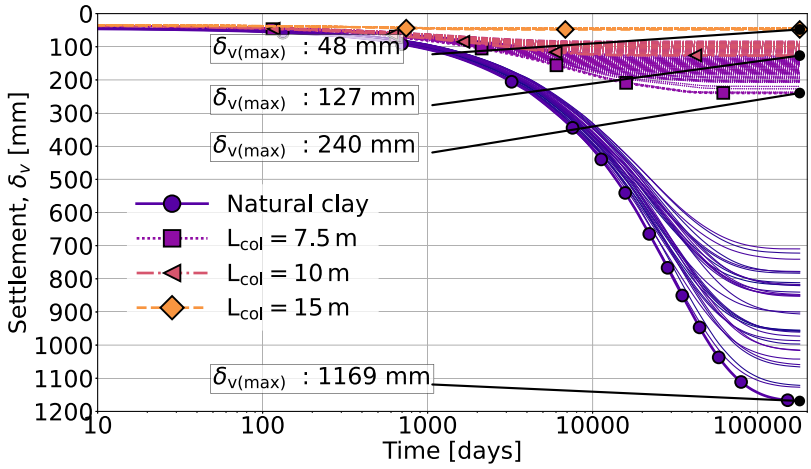

(a)

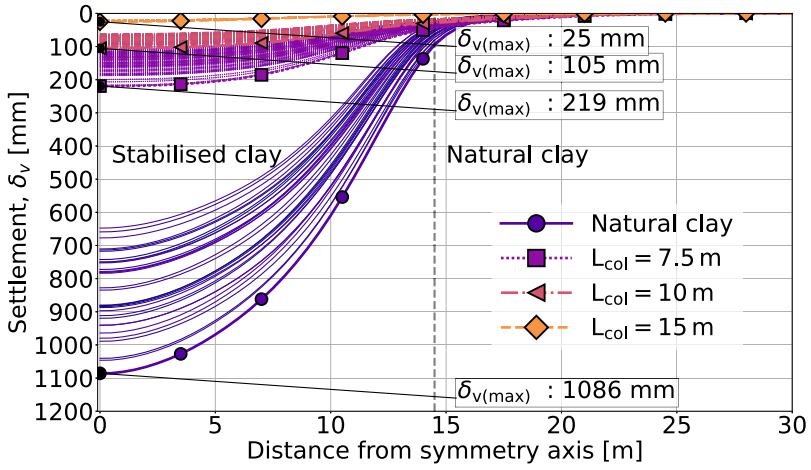

(b)

Fig. 5. Total settlement against time plots for natural clay (without stabilisation) (2_{IV}^{11-6}), stabilisation with 7.5 m long columns (2_{IV}^{18-11}), stabilisation with 10 m long columns (2_{IV}^{18-11}), and stabilisation with 15 m long columns (2_{IV}^{18-11}): (a) at the top of the embankment (Point A) (semi-logarithmic scale); (b) in the longitudinal direction at the surface of the soft clay (S-line).

using 7.5 m long columns was less effective than employing 10 m long columns in controlling the displacements (refer to Fig. 6), resulting in a greater rotation of principal stresses affecting the evolution of anisotropy in the unimproved soft clay (refer to Fig. E.11 in Appendix E). In Figs. 6 and E.11, the lower (–) and higher (+) boundaries, which result in the largest deformation and change in anisotropy, are displayed at the top of each case. For modelling the soft clay, adopting S-CLAY1S ensured accounting for the evolution of anisotropy due to plastic straining, thus providing a more realistic prediction of the stress–strain response.

After the investigation of the effect of the factors and the directions of their influence, to statistically assess the most influential parameters, the equality of the variances was examined using ANOVA. The F-test (for two-way or categorical ANOVA) is a statistical tool for testing the equality of independent population means at two levels on a dependent result. Its primary purpose is to determine whether there is a significant difference between the means of multiple groups.

The test results of the factorial designs are consistent with the main-effect plots. As an illustrative example, the fractional factorial design of the case without soil improvement is examined in Appendix A. For the unimproved case, the order of the most influential parameters identified with the variance analysis agrees with the main effect plot (refer to Fig. 4(a)). In Table A.7, the *p*-value indicates the probability of obtaining the observed differences that lead to the rejection of the equality of variances.

• *Interaction effects*

For a robust identification of influential parameters, the interaction effects must be assessed. Following a factorial design approach, performing FE simulations using a full factorial design is beneficial as it provides insights into the various interactions among two or more factors. The transition case with soil improvement using 10 m long columns, where the properties of the columns such as the stiffness and volume fraction begin to show significance, is chosen. Fig. 7 shows the results of a full factorial design for the case with 10 m long columns, including the plots of main effects, normality, and interaction effects.

The magnitude of the order and direction of the main effects computed by the full factorial design (in Fig. 7(a)) are comparable to those of the fractional factorial design (in Fig. 4(c)). However, the complete factorial design provides second-order interactions, as can be seen in Fig. 7(c). The second-order interactions are noticeable among the influential factors with an order of approximately 1–1.5 mm, which is less significant than the main effects. The factors associated

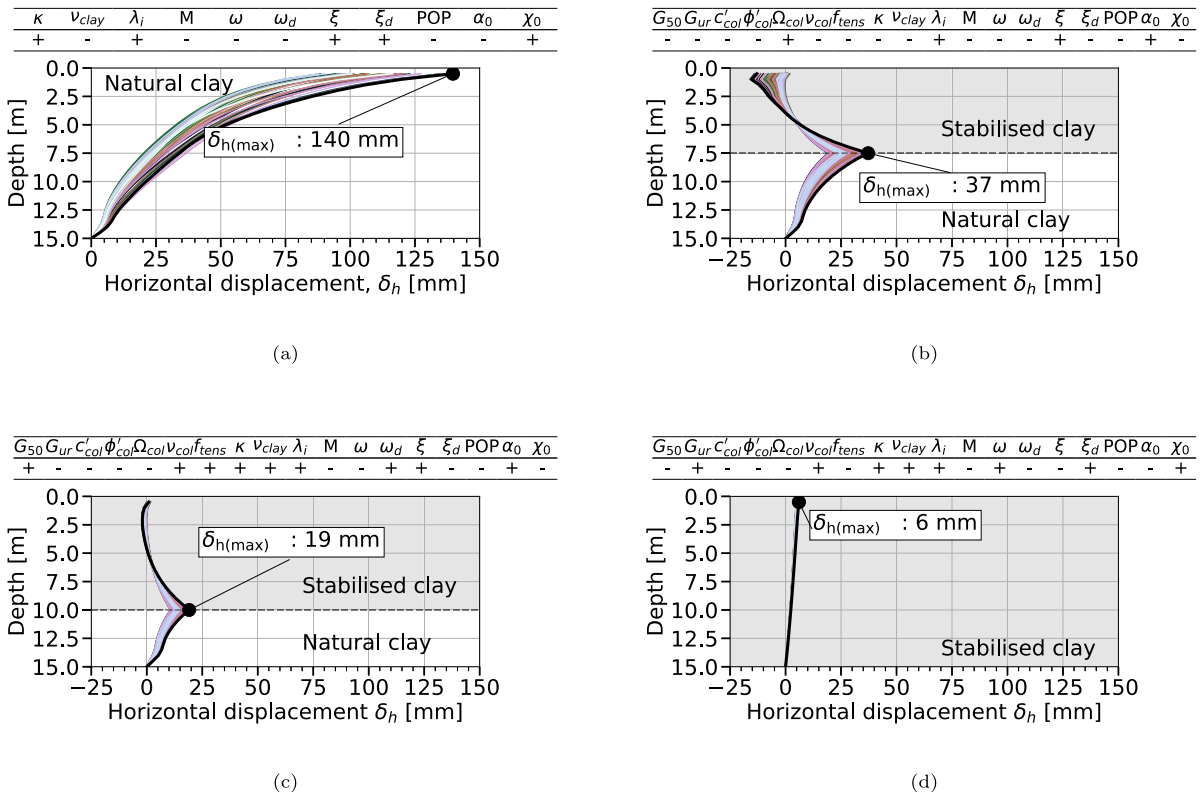

Fig. 6. Horizontal displacements calculated underneath the embankment (H-line) at the end of consolidation: (a) natural clay (without stabilisation) (2^{11-6}_{IV}); (b) stabilisation with 7.5 m long columns (2^{18-11}_{IV}); (c) stabilisation with 10 m long columns (2^{18-11}_{IV}); (d) stabilisation with 15 m long columns (2^{18-11}_{IV}).

with the individual materials (i.e. soft clay and the columns) remain largely independent. Additionally, the most influential parameters for this particular case can be distinguished in Fig. 7(b) as outliers. The inhomogeneity of variances for M, POP, λ_i, ξ, and α_0 becomes more pronounced with increasing levels of non-normality. The deviations from normality are of little concern when the primary target is to identify the factors having the greatest impact on the response rather than optimisation.

The direction of the effects of the main factors at two levels, with a factor difference of the same order, also controlled the direction of the interaction effects. The computed settlements decrease for the combined effect of the M and λ_i, whereas they increase for that of the λ_i and ξ. The latter implies that both factors individually elevate the compressibility of the natural clay, and their combined effect causes an increase in the average response. In contrast, the former suggests that the average settlement between the levels of M decreases when all levels of λ_i are considered. Yet, it is evident from Figs. 7(b) and 7(c) that the main effects have a greater influence on the computed response than the interaction effects.

The distribution of the maximum consolidation settlements computed at the top of the embankment is shown in Fig. 8 for the full factorial design. The plot displays the results for each factor at two levels (low: −1 and high: +1). The line in the middle of the box plots represents the median value (the second quartile, Q2). The first quartile (Q1) and the third quartile (Q3) indicate the 25th and 75th percentiles of the data, respectively, while the whiskers extend to the minimum and maximum values within ±1.5 times the interquartile range (IQR = Q3–Q1). As shown in Fig. 8, the median values of the most influential factors identified in the main effects plot (refer to Fig. 7(a)) lead to the highest values of maximum settlements, with the largest difference observed at different factor levels.

All sensitivity analyses were performed on a standard laptop PC equipped with an i5-1345U processor, a clockspeed of 1.2/4.7 GHz, along with 16 GB of memory. Table 4 shows the elapsed times for various design cases, including the scenario of unimproved natural clay and several configurations with different lengths of LC columns. The elapsed times, measured in hours, reflect the computational effort required for each case. The computational times vary considerably for the cases of 10 m columns, from 9.2 h for the fractional factorial design to 116.5 h for the full factorial scenario. This highlights the efficiency of the fractional factorial design in reducing computational demand while yielding comparable results, as demonstrated in Sections 3.2 and 4.1.

4.2. Baseline optimisation

In the application of DSM, the material manufacturing phase of the life cycle is the primary contributor to the environmental impacts [8,11]. According to 2018 data, the energy- and process-related emissions from cement production account for 34% and 66%, respectively [70]. The latter emissions mainly result from the calcination process of raw materials (e.g. limestone, chalk, clay) in the clinker-making process, from the combustion of fossil fuels in the kiln, and from electricity use during the production of cement [8] and lime [6]. Additionally, CO_2 emissions associated with DSM construction and equipment use raise environmental concerns. Despite efforts to reduce CO_2 emissions through measures, such as replacing clinker with alternative binders [71–73], capturing CO_2 from flue gases and utilising renewable energy sources instead of fossil fuels, the cement industry remains incompatible with zero-emissions targets set by the Paris Agreement [70].

Balancing the benefits of soil improvement using deep-mixing with environmental flows (e.g. energy use and CO_2 emissions), and ensuring cost efficiency (i.e. material use) during the design phase of infrastructure projects is therefore crucial. In the following section, the reference case of an embankment stabilised with LC columns was investigated to assess the total volume of LC use and the associated emissions from

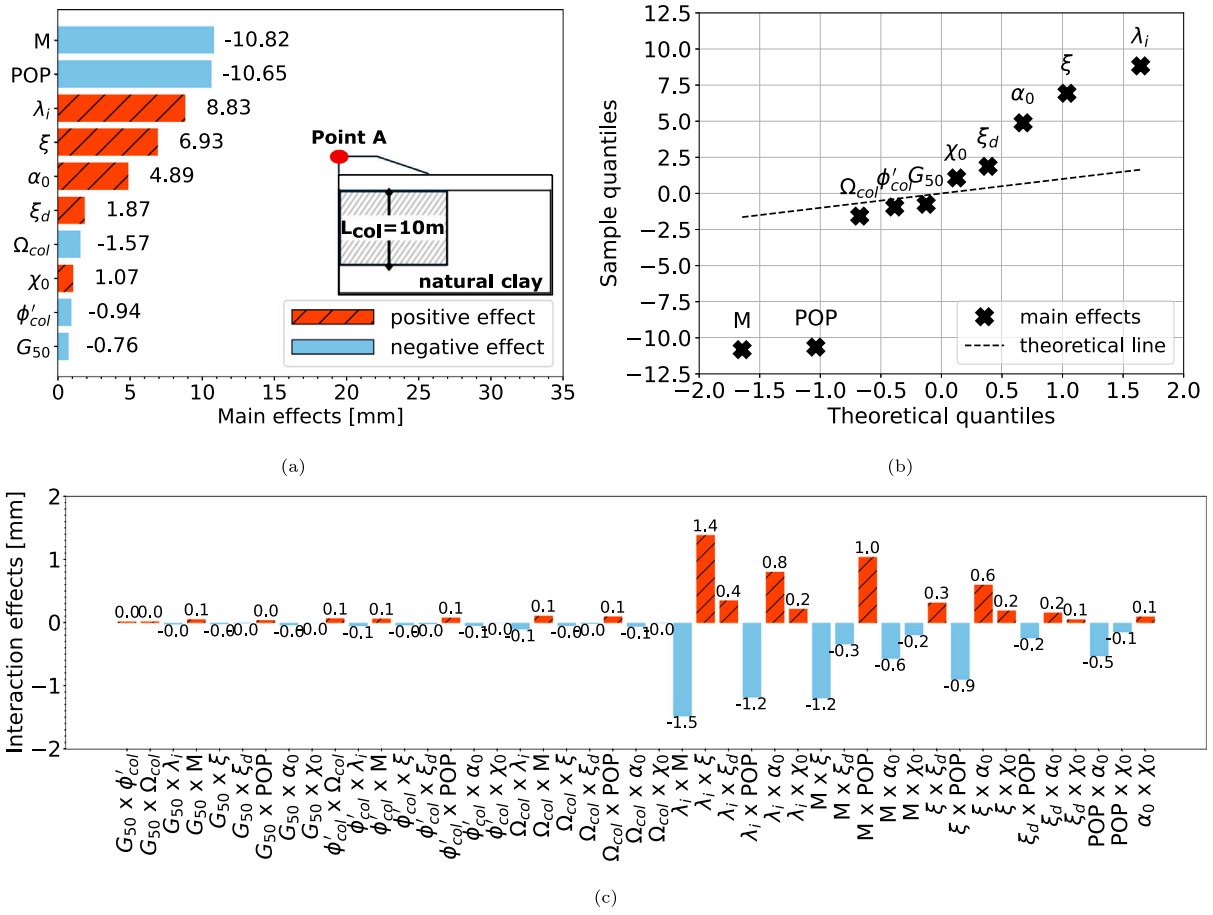

Fig. 7. Full factorial design for 10 m long columns (2^{10}): (a) main effects; (b) normality plot; (c) interaction effects.

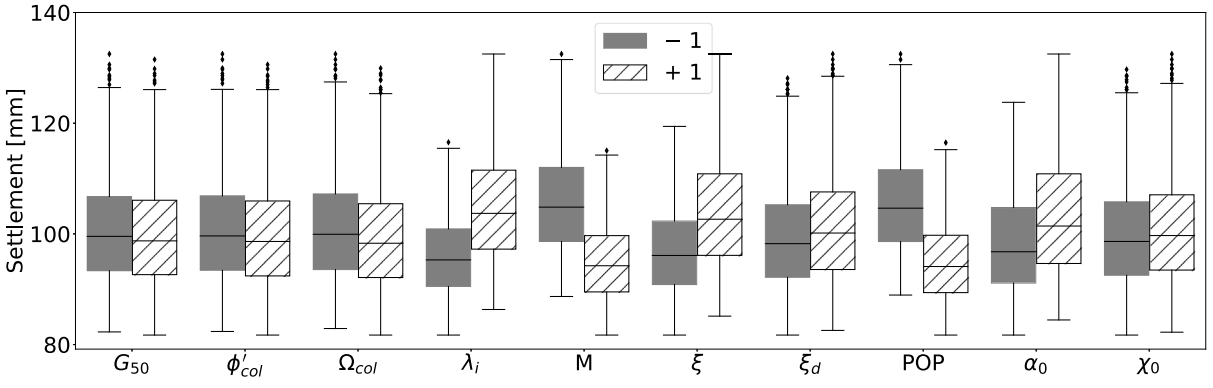

Fig. 8. Influence of upper and lower parameter values on settlement for the full factorial design using 10 m long columns (2^{10}).

Table 4
Elapsed time for factorial design cases.

Case	Factorial design	Total run	Elapsed time [hrs]
Unimproved case *in situ* clay	2^{11-6}_{IV}	32	2.3
Soil improvement with 7.5 m columns	2^{18-6}_{IV}	128	5.9
Soil improvement with 10 m columns	2^{18-6}_{IV}	128	9.2
Soil improvement with 15 m columns	2^{18-6}_{IV}	128	8.2
Soil improvement with 10 m columns	2^{10}	1024	116.5

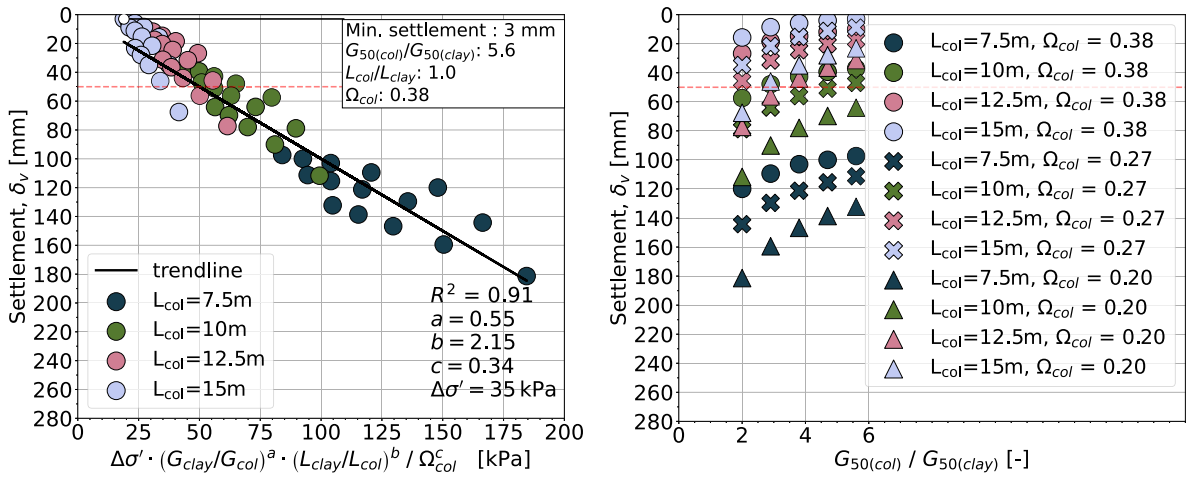

(a) (b)

Fig. 9. Dispersion of maximum settlement: (a) maximum settlement against $\Delta\sigma' \cdot (G_{clay}/G_{col})^a \cdot (L_{clay}/L_{col})^b / \Omega_{col}^c$ [kPa], (b) maximum settlement against $G_{50(col)}/G_{50(clay)}$.

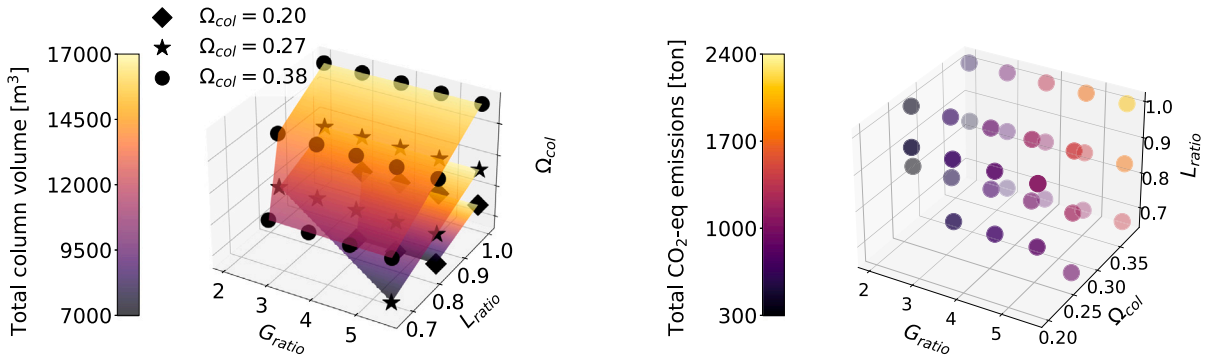

(a) (b)

Fig. 10. Variability in total column volume and corresponding total CO_2-eq emissions in relation to parameter variability of G_{ratio}-L_{ratio}-Ω_{col}: (a) surface plot of the total column volume; (b) scatter plot of the CO_2-eq emissions during the material production stage.

material production for a predefined tolerable maximum consolidation settlement. The assessment considers various design factors such as the volume fraction, the length of the LC columns, and the relative shear stiffness between the *in situ* natural clay and the columns.

• *How weak can the columns be?*

Incorporating DOE into the simulations provided distinct mechanisms between the floating and end-bearing columns that govern the long-term hydromechanical response, which helped to determine the most influential parameters. Yet, the link between the column stiffness and length, as well as the stabilised volume for SLS requires consideration of the site-specific ranges of the column stiffness which tend to show large variation due to the heterogeneity of the columns [67,74–76]. To perform a crude optimisation, such as estimating the approximate total volume of the columns and the material production-related CO_2 emissions, the volume fraction, and therefore the number and length of the columns, can be controlled by the designer, a simplified approach using OVAT can be adopted for a known (e.g. constant) load application. Thereby, the effect of the stiffness ratio G_{ratio} between the columns and clay can be assessed by considering the maximum settlement following the construction of a road embankment for an arbitrary consolidation period.

The influence of parameter variability on the maximum settlements, measured at the top of the embankment, was investigated using the same numerical model outlined in Section 2.1. A variety of shear moduli ($G_{50(col)}$) and lengths (L_{col}) for the columns, along with various stabilisation ratios based on different values of volume fraction Ω_{col}, were adopted. Throughout the analyses, the embankment load was kept constant at approximately 35 kPa. The range of L_{col} values is from 7.5 m to 15 m, with Ω_{col} values of 0.20, 0.27, and 0.38, corresponding to the column spacings of 1 m, 1.2 m, and 1.4 m, respectively. L_{clay} denotes the depth of the unimproved natural clay. The reference values of G_{50} for the columns, $G_{50(col)}$ and clay, $G_{50(clay)}$ are 28 MPa and 5 MPa, respectively. In the sensitivity studies, $G_{50(col)}$ varies between 10 MPa, 14.5 MPa, 19 MPa, 23.5 MPa, and 28 MPa, while $G_{50(clay)}$ remains constant.

In Figs. 9(a) and 9(b), the maximum settlements computed by the numerical model are presented. The consolidation settlements due to the embankment loading led to a power-law relationship with a coefficient of determination, R^2 of 0.91. As shown in Fig. 9(a), L_{col} has the most prominent influence on the calculated settlements, with the highest regression coefficient. However, the influence of G_{ratio} increases when either L_{col} or Ω_{col} decreases.

Fig. 9(b) suggests that to limit the settlements to less than a predefined tolerance (i.e. 50 mm), using less-rigid columns and/or shorter

Table 5
CO_2-eq emissions (kg CO_2-eq/ton) for different combinations yielding maximum and minimum emissions.

Combination	Component	Proportion (%)	Quantity (ton)	CO_2-eq emissions factor (kg CO_2-eq/ton)	Total CO_2-eq emissions (kg CO_2-eq)
Upper boundary	QL	50	921	1450[a]	1335076
G_{ratio} = 5.6 (110 kg/m^3)[b]	OPC	50	921	870[a]	801045
L_{col} = 15 m Ω_{col} = 0.38	Total	**100**	**1842**	**1842**	**2136121**
Lower boundary	QL	50	144	1450[a]	208422
G_{ratio}=2.0 (30 kg/m^3)[b]	OPC	50	144	870[a]	125053
L_{col} = 12.5 m Ω_{col} = 0.27	Total	**100**	**288**	**2320**	**333476**

[a] CO_2-eq emissions factors are based on Klimatkalkyl version 7.0 by Trafikverket (Swedish Transport Administration).
[b] Binder contents corresponding to target stiffness moduli are estimated based on [36].

columns is a viable option. The 15 m long end-bearing and 12.5 m long floating columns allowed for the potential use of less-rigid columns, suggesting that $G_{50(col)}$ can be reduced by approximately threefold. Meanwhile, using 10 m long columns necessitated adopting an Ω_{col} value higher than 0.27 or the G_{50} ratio exceeding 2.9. When 50 mm is selected as the tolerable settlement, employing the 7.5 m long columns would not be sufficient by any means.

The results of the OVAT simulations revealed that the length and stiffness of the columns are highly influential for the hypothetical case. However, to account for the variability in natural clay, as demonstrated in Section 4.1, especially for cases with floating columns, DOE can be employed using site-specific ranges of the parameters to quantify the induced uncertainty or to perform realistic optimisation.

• *Climate impact*

The climate impact originating from the overall carbon dioxide equivalent, CO_2-eq emissions associated solely with the material production can be estimated by computing the approximate total volume of the LC columns. The results of the sensitivity analyses from the OVAT analyses above were adopted for a crude estimate.

In Fig. 10(a), several total volumes of columns are presented for a tolerable limit settlement of 50 mm, following the construction of the embankment. The combinations of Ω_{col} and the relative ratios of the moduli, G_{ratio} and lengths, L_{ratio} between the clay and columns are adopted, where $G_{ratio} = G_{50(col)}/G_{50(clay)}$ and $L_{ratio} = L_{col}/L_{clay}$. The number of columns is computed for a representative section of 100 m. Subsequently, the corresponding CO_2-eq emissions are calculated for the volumes associated with different G_{ratio}, L_{ratio}, and Ω_{col} (in Fig. 10(b)).

The relationship between the strength and stiffness of stabilised clays are well correlated [75,77,78], although it may vary depending on several factors such as clay composition (e.g. inorganic and organic), binder type/composition, binder content (kg/m^3), binder proportion, curing period, curing condition, the weight ratio of water and cementitious material (w/c), the weight ratio of soil and cementitious material (s/c), mixing technique (wet or dry) and mixing procedure (i.e. the number of blades on the mixing tool, retrieval rate and rotation speed [66]). The relationship has been extensively studied in the Nordic countries by comparing the results of field and laboratory tests using DSM [i.e. 36,76,79–82] or the modified deep mixing or the wet mixing method [i.e. 72,83]. International sources referring to the wet mixing method [e.g. 84,85] include studies focused on the small strain region [e.g. 86–88]. An increase in the binder content leads to an increase in the undrained strength, c_u and the stiffness obtained from laboratory (i.e. uniaxial compression, vane, triaxial) or field tests (i.e. bender element, resonant column, piezocone, column penetration (FKPS/ FOPS)).

CO_2-eq emissions caused by the production of quick lime (QL) and Ordinary Portland Cement (OPC) can be calculated by multiplying an emission factor by the quantity of materials used. The ratio between the secant modulus, E_{50}, at a deviator stress level of 50% of the unconfined compressive strength, q_u, to q_u, can be roughly estimated based on [76, 82]. In this study, E_{50}/q_u is taken as 133. The calculation assumes that q_u increases with the binder content, using the values suggested by [36] based on the Nordic experience. In the Nordic countries, the traditional binders for inorganic clays include OPC and QL, typically applied at 70–120 kg/m^3 of soil [82,89]. The adopted binder contents range between 30 and 110 kg/m^3 to achieve the target $G_{50(col)}$ using elastic theory ($G = E_u/(2(1+\nu_u))$) for a fixed binder ratio of 50:50 (50% OPC and 50% QL).

The computed emissions (kg CO_2-eq/ton) for various combinations that result in maximum and minimum emissions to achieve the tolerable settlement are shown in Table 5. Using the end-bearing columns of 15 m with the upper boundary of Ω_{col} and G_{ratio} (0.38 and 5.6, respectively) led to the highest emissions, while the 12.5 m long columns produced the lowest emissions with a Ω_{col} of 0.27 and G_{ratio} of 2.0. Notably, the different configurations of both the floating and end-bearing columns enabled a reduction in the column stiffness by approximately threefold.

5. Conclusions

The time-dependent hydromechanical response of an embankment on soft natural clay stabilised by lime-cement (LC) columns was investigated to identify the most influential factors for Serviceability Limit State. The non-linear responses of both the *in situ* clay and the columns were taken into account in a plane strain analysis using the volume averaging technique (VAT). The incorporation of two constitutive soil models describing the response of each constituent (clay and the columns) allowed for identifying the most influential material parameters, which evolve as a function of time due to the dissipation of pore pressures. The presented systematic approach using the Design of Experiments (DOE) enabled identifying the governing mechanism and related factors having the largest impact on the stress–strain response, with reduced computational demand.

A series of simulations were performed on various stabilisation ratios, soil model parameters, and length configurations, including end-bearing and floating columns using the factorial design. The results showed that the parameters of the soft clay significantly affect the computed deformations when using floating columns, compared to end-bearing columns. The order of deformations and the magnitude of stress rotations decreased with increasing LC column length, while the column stiffness became more significant in the response for the end-bearing columns. Additionally, the link between the column length, stabilisation ratio, and the relative stiffness between the clay and the columns revealed the possibility of using less rigid columns in field applications to achieve a tolerable settlement as per project requirements. The latter approach, however, leads to smaller differences between the stiffness in the columns and the surrounding soil, which necessitates the use of high-fidelity numerical models that include the non-linear response of the clay and column material.

This study highlights that the presented systematic approach, using VAT in combination with DOE, can be adapted to perform sensitivity analyses and/or data-driven procedures in a plane strain analysis efficiently. Considering the parameter variability of LC columns due to heterogeneity, incorporating site-specific ranges and spatial variability in the analyses can provide realistic predictions of the soil response, resulting in reduced maintenance costs in the future and, as shown in this work, potentially a lower climate impact.

CRediT authorship contribution statement

Sinem Bozkurt: Writing – original draft, Methodology, Writing – review & editing, Software, Conceptualization, Visualization, Formal analysis. **Jelke Dijkstra:** Writing – review & editing, Supervision. **Minna Karstunen:** Supervision, Writing – review & editing, Funding acquisition, Project administration.

Declaration of competing interest

The authors declare that they have no known competing financial interests or personal relationships that could have appeared to influence the work reported in this paper.

Acknowledgements

The work received financial support from BIG (Better Interaction in Geotechnics, Grant 2020/46703 and TRV 2024/27461) through the Swedish Transport Administration (TRV) and Formas (Swedish Research Council for Sustainable Development, Grant 2019-00456). The work is a part of the Digital Twin Cities Centre that is supported by Sweden's Innovation Agency VINNOVA (Grant 2024-03904).

Appendix A. Fractional factorial design

The fractional factorial design table of contrast for the unimproved case is shown in Table A.6 with each factor at two levels. High and low

Table A.6
2^{11-6}_{IV} fractional factorial design: table of contrast for the natural clay.

	A	B	C	D	E	F = ABC	G = ABD	H = ABE	I = ACD	J = ACE	K = ADE
Run	κ	ν_{clay}	λ_i	M	ω	ω_d	ξ	ξ_d	POP	α_0	χ_0
1	−	−	−	−	−	−	−	−	−	−	−
2	+	−	−	−	−	+	+	+	+	+	+
3	−	+	−	−	−	+	+	+	−	−	−
4	+	+	−	−	−	−	−	−	+	+	+
5	−	−	+	−	−	+	−	−	+	+	−
6	+	−	+	−	−	−	+	+	−	−	+
7	−	+	+	−	−	−	+	+	+	+	−
8	+	+	+	−	−	+	−	−	−	−	+
9	−	−	−	+	−	−	+	−	+	−	+
10	+	−	−	+	−	+	−	+	−	+	−
11	−	+	−	+	−	+	−	+	+	−	+
12	+	+	−	+	−	−	+	−	−	+	−
13	−	−	+	+	−	+	+	−	−	+	+
14	+	−	+	+	−	−	−	+	+	−	−
15	−	+	+	+	−	−	−	+	−	+	+
16	+	+	+	+	−	+	+	−	+	−	−
17	−	−	−	−	+	−	−	+	−	+	+
18	+	−	−	−	+	+	+	−	+	−	−
19	−	+	−	−	+	+	+	−	−	+	+
20	+	+	−	−	+	−	−	+	+	−	−
21	−	−	+	−	+	+	−	+	+	−	+
22	+	−	+	−	+	−	+	−	−	+	−
23	−	+	+	−	+	−	+	−	+	−	+
24	+	+	+	−	+	+	−	+	−	+	−
25	−	−	−	+	+	−	+	+	+	+	−
26	+	−	−	+	+	+	−	−	−	−	+
27	−	+	−	+	+	+	−	−	+	+	−
28	+	+	−	+	+	−	+	+	−	−	+
29	−	−	+	+	+	+	+	+	−	−	−
30	+	−	+	+	+	−	−	−	+	+	+
31	−	+	+	+	+	−	−	−	−	−	−
32	+	+	+	+	+	+	+	+	+	+	+

Table A.7
Analysis of variance: FE simulations using fractional factorial design for the natural clay (without stabilisation) (2^{11-6}_{IV}).

Source of variation	Sum of squares	Degrees of freedom	F_0	p-value
λ_i	215 625.80	1	1119.56	< 0.0001
ξ	101 408.70	1	526.53	< 0.0001
M	98 715.69	1	512.555	< 0.0001
POP	30 136.97	1	156.48	< 0.0001
α_0	13 240.93	1	68.75	< 0.0001
ξ_d	8814.27	1	45.76	< 0.0001
χ_0	5901.60	1	30.64	< 0.0001
κ	833.44	1	4.33	0.05
ω_d	504.11	1	2.62	0.12
ω	317.08	1	1.65	0.21
ν_{clay}	2.32	1	0.01	0.91
residual	3851.98	20	8.4	10.6

Table D.8
Model parameters for dry crust.

Material model	γ_n (kN/m^3)	E'^{ref}_{50} (kPa)	E'^{ref}_{oed} (kPa)	E'^{ref}_{ur} (kPa)	m	p^{ref} (kPa)	c' (kPa)	ϕ' (°)	K_0
HS (Undrained A)	16.5	7200	7200	21 600	0.5	100	2	35	0.94

Table D.9
Model parameters for embankment fill.

Material model	γ_n (kN/m^3)	E' (kPa)	ν' (-)	c' (kPa)	ϕ' (°)	K_0
MC (Drained)	20	40 000	0.3	1	35	0.43

levels are denoted by "+" and "−", respectively. Design generators of 2^{11-6}_{IV} fractional factorial design are F = ABC, G = ABD, H = ABE, I = ACD, J = ACE and K = ADE which construct the design resolution of the experiment as IV based on the smallest word with three letters in the defining relation, **I**.

where,

$$\begin{aligned}\mathbf{I} &= \text{ABCF} = \text{ABDG} = \text{ABEH} = \text{ACDI} = \text{ACEJ} = \text{ADEK} = \text{CFDG}\\ &= \text{ABCDI} = \text{ABCEJ}\\ &= \text{ABCFDEK} = \text{ABEGH} = \text{ABCDGI} = \text{ABDEJ} = \text{ABEHCDI}\\ &= \text{ABEHCEJ} = \text{ABEHDEK}\\ &= \text{ACDIJ} = \text{ACDFE} = \text{ACEJDEK} = \text{ABCFDEG} = \text{ABCDHI}\\ &= \text{ABDEJK} = \text{ABHECDI}\\ &= \text{ABHEDEK} = \text{ABEHJDEK} = \text{ABCDJK} = \text{ACDEJ} = \text{ABCDG}\\ &= \text{ABDE} = \text{ABFJ} = \text{ABHEK}\\ &= \text{ABHJK} = \text{ABCDE} = \text{ABEJ} = \text{ABEK} = \text{ABJDE} = \text{ACDIJK}\\ &= \text{ABFDE} = \text{ABHECDK}\end{aligned} \tag{A.1}$$

Therefore, main effects are confounded with three-factor interactions (joint effect of three factors), and two-factor interactions (joint effect of two factors) are confounded with other two-factor interactions.

Appendix B. Formulation of S-CLAY1S

The yield surface equation of the S-CLAY1S model [34,38] in generalised stress states is expressed as follows:

$$f_{3D} = \underbrace{\frac{3}{2}\left(\left\{\sigma'_d - p'\alpha_d\right\}^T\left\{\sigma'_d - p'\alpha_d\right\}\right)}_{q^2} - \left(M^2 - \underbrace{\frac{3}{2}\left\{\alpha_d\right\}^T\left\{\alpha_d\right\}}_{\alpha^2}\right)\times \left(p'_m - p'\right)p' = 0 \tag{B.1}$$

where q is the scalar value of the modified deviatoric stress tensor, including anisotropy represented by a deviatoric fabric tensor α_d. $q = (\sigma'_1 - \sigma'_3)$ in triaxial stress space. Mean effective stress is $p' = (\sigma'_1 + \sigma'_2 + \sigma'_3)/3$ and the vertical tangent to natural yield surface designates the size in the isotropic axis, p'_m. M represents the stress ratio at the critical state. The subscript scalar value of the fabric tensor denotes α, which describes the orientation of the model surfaces.

The three hardening laws used in the model define the changes in the size of the intrinsic yield surface, the progressive loss of bonding and the rotation of the yield surface. The size of the intrinsic yield surface, p'_{mi} is assumed to be dependent only on volumetric plastic strains, ε^p_v.

$$\Delta p'_{mi} = \frac{(1+e)\,p'_{mi}}{\lambda_i - \kappa}\Delta\varepsilon^p_v \tag{B.2}$$

The evolution of the size of p'_m, corresponding to the current degree of bonding (χ), and the degradation of bonding are calculated with Eq. (B.3). The Macaulay brackets, $\langle\rangle$ are used to impose $\Delta\varepsilon^p_v = \Delta\varepsilon^p_v$ for $\Delta\varepsilon^p_v > 0$ and $\Delta\varepsilon^p_v = 0$ for $\Delta\varepsilon^p_v < 0$.

$$\Delta\chi = -\xi\chi\left(\left\langle\Delta\varepsilon^p_v\right\rangle + \xi_d\Delta\varepsilon^p_d\right) \text{ and } p'_m = (p'_{mi} + \Delta p'_{mi})(1 + (\chi + \Delta\chi)) \tag{B.3}$$

The evolution of anisotropy is described with Eq. (B.4) in 3D stress space.

$$\Delta\alpha = \omega\left[\left(\frac{3\sigma'_d}{4p'} - \alpha_d\right)\left\langle\Delta\varepsilon^p_v\right\rangle + \omega_d\left(\frac{\sigma'_d}{3p'} - \alpha_d\right)\Delta\varepsilon^p_d\right] \tag{B.4}$$

Appendix C. Formulation of MNhard

The yield surface equation of the Matsuoka–Nakai hardening (MNhard) model [35] is expressed as follows:

$$f_s = \frac{3}{4}\frac{q_a}{E'_{50}}\frac{q}{q_a - q} - \frac{3}{2}\frac{2q}{E'_{ur}} - \gamma^{ps}_s \text{ and } R_f = \frac{q_f}{q_a} < 1.0 \tag{C.1}$$

where the secant and unloading–reloading stiffnesses are defined by E'_{50} and E'_{ur} (refer to Eq. (C.2)), while γ^{ps}_s describes the accumulated deviatoric plastic shear strain, γ^{ps}_s. q_a, q_f, and R_f are the asymptotic deviatoric stress, the deviatoric stress at failure and the failure ratio.

$$E'_{50,ur} = E'^{ref}_{50,ur}\left(\frac{\sigma'_3 + c'\cot\phi'}{\sigma'^{ref} + c'\cot\phi'}\right)^m \tag{C.2}$$

where E'^{ref}_{50} and E'^{ref}_{ur} are the reference secant and unloading–reloading moduli corresponding to a reference effective stress, σ'^{ref}. σ'_3 is the minor effective stress, and the exponent of m is a model parameter that reflects the stress-dependency of the stiffness of the material. The model parameter of the shear modulus, G can be computed using the effective Poisson's ratio, ν' based on elasticity theory.

Appendix D. Soil model parameters for dry crust and embankment fill

See Tables D.8 and D.9.

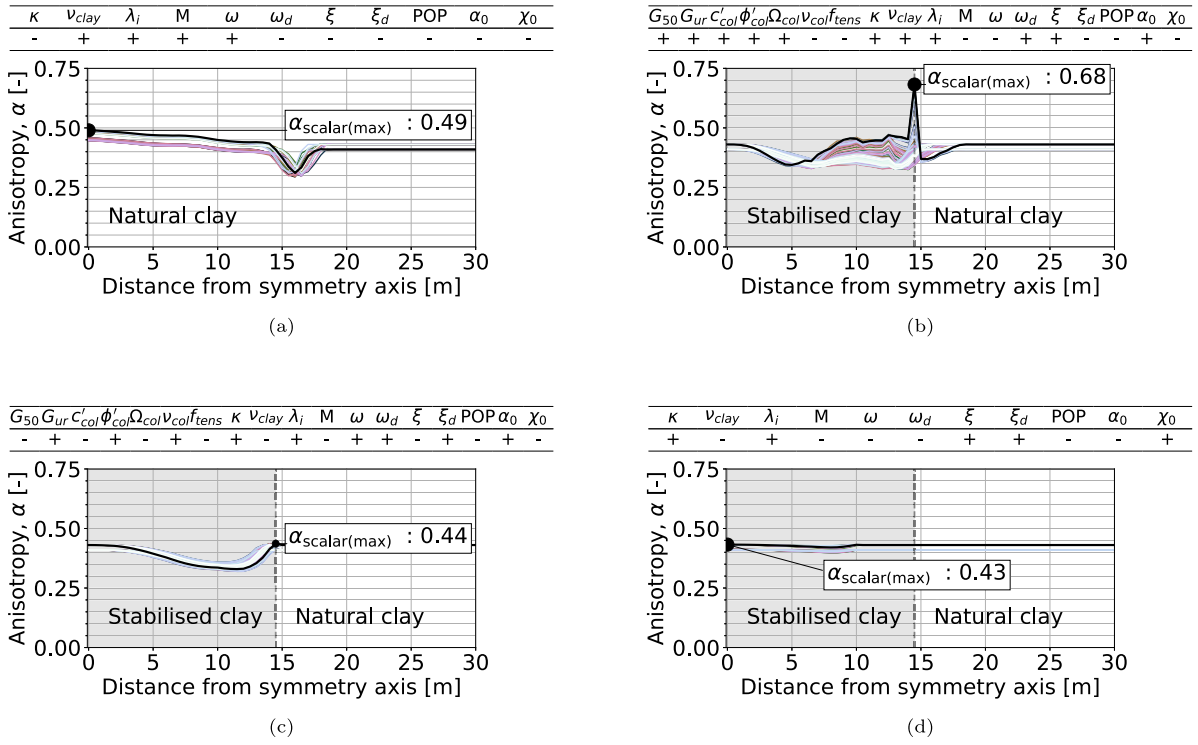

Fig. E.11. Scalar value of anisotropy calculated underneath the embankment in the longitudinal direction (H-line) after 500 years: (a) natural clay (without stabilisation) (2^{11-6}_{IV}); (b) stabilisation with 7.5 m long columns (2^{18-11}_{IV}); (c) stabilisation with 10 m long columns (2^{18-11}_{IV}); (d) stabilisation with 15 m long columns (2^{18-11}_{IV}).

Appendix E. Change in anisotropy

See Fig. E.11.

Data availability

Data will be made available on request.

References

[1] SS-EN:197-1. Part 1: Compositions, specifications and conformity criteria for common cements. European Committee for Standardization EN, 197–1; 2011.

[2] Holm G, Andréasson B, Bengtsson PE, Bodare A, Eriksson H. Mitigation of track and ground vibrations by high speed trains at Ledsgard, Sweden. Report 10, Swedish Deep Stabilization Research Centre; 2002, p. 58–67.

[3] Larsson S. The mixing process at the dry jet mixing method. In: Dry mix methods for deep soil stabilization. Routledge; 2017, p. 339–46.

[4] Holt DGA, Jefferson I, Braithwaite PA, Chapman DN. Sustainable geotechnical design. In: GeoFlorida 2010: Advances in analysis, modeling and design. Chapter. 2010, p. 2925–32. http://dx.doi.org/10.1061/41095(365)298.

[5] Oates J. Production of quicklime. chapter 16, John Wiley & Sons, Ltd.; 1998, p. 155–91. http://dx.doi.org/10.1002/9783527612024.ch16.

[6] Simoni M, Wilkes MD, Brown S, Provis JL, Kinoshita H, Hanein T. Decarbonising the lime industry: State-of-the-art. Renew Sustain Energy Rev 2022;168:112765. http://dx.doi.org/10.1016/J.RSER.2022.112765.

[7] Taylor H. Cement chemistry. 2nd ed.. Thomas Telford Publishing; 1997, http://dx.doi.org/10.1680/cc.25929.

[8] Worrell E, Price L, Martin N, Hendriks C, Meida LO. Carbon dioxide emissions from the global cement industry. Annu Rev Environ Resour 2001;26:303–29. http://dx.doi.org/10.1146/annurev.energy.26.1.303.

[9] IEA. Energy technology perspectives 2023. Technical Report, France: International Energy Agency; 2023, URL: https://iea.blob.core.windows.net/assets/a86b480e-2b03-4e25-bae1-da1395e0b620/EnergyTechnologyPerspectives2023.pdf.

[10] Menzies GF, Turan S, Banfill PFG. Life-cycle assessment and embodied energy: A review. Proc Inst Civ Eng - Constr Mater 2007;160:135–43. http://dx.doi.org/10.1680/coma.2007.160.4.135.

[11] Raymond AJ, DeJong JT, Alissa K, Blackburn JT, Rick D. Life cycle sustainability assessment of geotechnical ground improvement methods. J Geotech Geoenvironmental Eng 2021;147:04021161. http://dx.doi.org/10.1061/(ASCE)GT.1943-5606.0002646.

[12] ISO 14040. Environmental management - life cycle assessment - principles and framework. Geneva, Switzerland: International Organization for Standardization; 2006.

[13] Samuelsson I, Spross J, Larsson S. Integrating life-cycle environmental impact and costs into geotechnical design. Proc Inst Civ Eng: Eng Sustain 2023;177:19–30. http://dx.doi.org/10.1680/jensu.23.00012.

[14] Shillaber CM, Mitchell JK, Dove JE. Energy and carbon assessment of ground improvement works. I: Definitions and background. J Geotech Geoenvironmental Eng 2016;142:04015083. http://dx.doi.org/10.1061/(ASCE)GT.1943-5606.0001410.

[15] Shillaber CM, Mitchell JK, Dove JE. Energy and carbon assessment of ground improvement works. II: Working model and example. J Geotech Geoenvironmental Eng 2016;142. http://dx.doi.org/10.1061/(ASCE)GT.1943-5606.0001411.

[16] Mohammed MA, Yunus NZM, Hezmi MA, Hasbollah DZA, Rashid ASA. Ground improvement and its role in carbon dioxide reduction: A review. Environ Sci Pollut Res 2021;28:8968–88. http://dx.doi.org/10.1007/s11356-021-12392-0.

[17] Behrens ILC. Overview of low-volume roads: Keynote address. Transp Res Rec 1999;1652:1–4. http://dx.doi.org/10.3141/1652-01.

[18] IEA. Technology roadmap: Low-carbon transition in the cement industry. Technical Report, Paris: International Energy Agency; 2018, URL: https://www.iea.org/reports/technology-roadmap-low-carbon-transition-in-the-cement-industry.

[19] Swedish Transport Administration. The Swedish transport administration's implementation plan for the years 2019–2024. Technical Report, Swedish Transport Administration; 2019, URL: http://trafikverket.diva-portal.org/smash/get/diva2:1363299/FULLTEXT01.pdf.

[20] Zdravkovic L, Potts DM, Hight DW. The effect of strength anisotropy on the behaviour of embankments on soft ground. Géotechnique 2002;52:447–57. http://dx.doi.org/10.1680/GEOT.2002.52.6.447.

[21] Indraratna B, Redana IW. Numerical modeling of vertical drains with smear and well resistance installed in soft clay. Can Geotech J 2000;37:132–45. http://dx.doi.org/10.1139/t99-115.

[22] Yapage NNS, Liyanapathirana DS, Kelly RB, Poulos HG, Leo CJ. Numerical modeling of an embankment over soft ground improved with deep cement mixed columns: Case history. J Geotech Geoenvironmental Eng 2014;140:04014062. http://dx.doi.org/10.1061/(ASCE)GT.1943-5606.0001165.

[23] Amavasai A, Sivasithamparam N, Dijkstra J, Karstunen M. Consistent class A & C predictions of the Ballina test embankment. Comput Geotech 2018;93:75–86. http://dx.doi.org/10.1016/J.COMPGEO.2017.05.025.

[24] Jaksa MB, Goldsworthy JS, Fenton GA, Kaggwa WS, Griffiths DV, Kuo YL, et al. Towards reliable and effective site investigations. Géotechnique 2005;55:109–21. http://dx.doi.org/10.1680/geot.2005.55.2.109.

[25] Ching J, Phoon KK, Yu JW. Linking site investigation efforts to final design savings with simplified reliability-based design methods. J Geotech Geoenvironmental Eng 2014;140:04013032. http://dx.doi.org/10.1061/(ASCE)GT.1943-5606.0001049.

[26] Vardon PJ, Liu K, Hicks MA. Reduction of slope stability uncertainty based on hydraulic measurement via inverse analysis. Georisk: Assess Manag Risk Eng Syst Geohazards 2016;10:223–40. http://dx.doi.org/10.1080/17499518.2016.1180400.

[27] Spross J, Bergman N, Larsson S. Reliability-based verification of serviceability limit states of dry deep mixing columns. J Geotech Geoenvironmental Eng 2021;147. http://dx.doi.org/10.1061/(asce)gt.1943-5606.0002458.

[28] Schweiger HF, Pande G N. Numerical analysis of a road embankment constructed in soft clay stabilised with stone columns. In: Proceedings of the sixth international conference on numerical methods in geomechanics, Innsbruck, 11-15 April. 1988, p. 1329–33.

[29] Lee JS, Pande GN. Analysis of stone-column reinforced foundations. Int J Numer Anal Methods Geomech 1998;22:1001–20. http://dx.doi.org/10.1002/(SICI)1096-9853(199812)22:12<1001::AID-NAG955>3.0.CO;2-I.

[30] Vogler U, Karstunen M. Application of volume averaging technique in numerical modelling of deep mixing. In: Geotechnics of soft soils: Focus on ground improvement. CRC Press; 2008, p. 201–8.

[31] Bozkurt S, Abed A, Karstunen M. Homogenisation method for braced excavations stabilised with deep-mixed columns. Comput Geotech 2025;181:107095. http://dx.doi.org/10.1016/j.compgeo.2025.107095.

[32] Abed A, Vogler U, Karstunen M. Volume averaging technique for deep mixed columns under embankments: Verification and validation. ASCE Int J Geomech 2025. [Accepted for publication].

[33] Box GEP, Hunter JS, Hunter WG. Statistics for experimenters: Design, innovation, and discovery. In: Wiley series in probability and statistics. 2nd ed.. Hoboken, N.J: Wiley-Interscience; 2005.

[34] Karstunen M, Krenn H, Wheeler SJ, Koskinen M, Zentar R. Effect of anisotropy and destructuration on the behavior of Murro test embankment. Int J Geomech 2005;5:87–97. http://dx.doi.org/10.1061/(asce)1532-3641(2005)5:2(87).

[35] Benz T. Small-strain stiffness of soils and its numerical consequences, vol. 5. Univ. Stuttgart, Inst. F. Geotechnik Stuttgart; 2007.

[36] Paniagua P, Bache BKF, Lund AK, Karlsrud K. Full-scale field-testing of lime-cement columns in a very sensitive clay. IOP Conf Ser: Earth Environ Sci 2021;710:012049. http://dx.doi.org/10.1088/1755-1315/710/1/012049.

[37] Bozkurt S, Abed A, Karstunen M. Finite element analysis for a deep excavation in soft clay supported by lime-cement columns. Comput Geotech 2023;162:105687. http://dx.doi.org/10.1016/j.compgeo.2023.105687.

[38] Koskinen M, Karstunen M, Wheeler SJ. Modelling destructuration and anisotropy of a soft natural clay. In: Mestat P, editor. Proceedings of the 5th European conf. numerical methods in geotechnical engineering. Paris: Presses de l'ENPC/LCPS; 2002, p. 11–20.

[39] Matsuoka H, Nakai T. Stress-deformation and strength characteristics of soil under three different principal stresses. In: Proceedings of the Japan society of civil engineers. Japan Society of Civil Engineers; 1974, p. 59–70.

[40] Matsuoka H, Nakai T. Relationship among Tresca, Mises, Mohr–Coulomb and Matsuoka–Nakai failure criteria. Soils Found 1985;25:123–8. http://dx.doi.org/10.3208/s{andf}1972.25.4_123.

[41] Gras JP, Sivasithamparam N, Karstunen M, Dijkstra J. Strategy for consistent model parameter calibration for soft soils using multi-objective optimisation. Comput Geotech 2017;90:164–75. http://dx.doi.org/10.1016/J.COMPGEO.2017.06.006.

[42] Gras JP, Sivasithamparam N, Karstunen M, Dijkstra J. Permissible range of model parameters for natural fine-grained materials. Acta Geotech 2018;13:387–98. http://dx.doi.org/10.1007/S11440-017-0553-1.

[43] Schanz T, Vermeer PA, Bonnier PG. The hardening soil model: Formulation and verification. 1999, p. 281–96. http://dx.doi.org/10.1201/9781315138206-27.

[44] SGF. Lime and lime cement columns. Guide for design, construction and control. Report 2:2000, Linköping, Sweden: Svenska Geotekniska Föreningen (Swedish Geotechnical Society; 2000 [in Swedish].

[45] Euro-Soil-Stab. Development of design and construction methods to stabilize soft organic soils: Design guide for soft soil stabilization. CT97-0351, Brysel: European Commission, Industrial and Materials Technologies Programme (Rite-EuRam III); 2002.

[46] Bruce MEC, Berg RR, Filz GM, Terashi M, Yang DS, Collin JG. Federal highway administration design manual: Deep mixing for embankment and foundation support. Technical Report FHWA-HRT-13-046, United States Federal Highway Administration; 2013, URL: https://rosap.ntl.bts.gov/view/dot/37379.

[47] Broms BB, Boman P. Lime columns—A new foundation method. J Geotech Eng Div 1979;105:539–56. http://dx.doi.org/10.1061/AJGEB6.0000788.

[48] Carlsten P. Lime and lime/cement columns. In: Hartlén J, Wolski W, editors. Embankments on organic soils. Developments in geotechnical engineering, vol. 80, Elsevier; 1996, p. 355–99. http://dx.doi.org/10.1016/S0165-1250(96)80013-7.

[49] Bergado DT, Ruenkrairergsa T, Taesiri Y, Balasubramaniam AS. Deep soil mixing used to reduce embankment settlement. Proc Inst Civ Eng - Ground Improv 1999;3:145–62. http://dx.doi.org/10.1680/GI.1999.030402.

[50] Rampello S, Callisto L. Predicted and observed performance of an oil tank founded on soil-cement columns in clayey soils. Soils Found 2003;43:229–41. http://dx.doi.org/10.3208/SANDF.43.4_229.

[51] Jiang Y, Han J, Zheng G. Numerical analysis of consolidation of soft soils fully-penetrated by deep-mixed columns. KSCE J Civ Eng 2013;17:96–105. http://dx.doi.org/10.1007/S12205-013-1641-X/METRICS.

[52] Kitazume M. Deep mixing technology – diversity and future development –. Jpn Geotech Soc Spec Publ 2024;11:1–16. http://dx.doi.org/10.3208/JGSSP.VOL11.KL-1.

[53] Graham J. Embankment stability on anisotropic soft clays. Can Geotech J 1979;16:295–308. http://dx.doi.org/10.1139/t79-031.

[54] Sloan SW. Substepping schemes for the numerical integration of elastoplastic stress–strain relations. Internat J Numer Methods Engrg 1987;24:893–911. http://dx.doi.org/10.1002/nme.1620240505.

[55] Vogler U. Numerical modelling of deep mixing with volume averaging technique (Ph.D. thesis), The University of Strathclyde; 2009.

[56] Alamgir M, Miura N, Poorooshasb HB, Madhav MR. Deformation analysis of soft ground reinforced by columnar inclusions. Comput Geotech 1996;18:267–90. http://dx.doi.org/10.1016/0266-352X(95)00034-8.

[57] Oliveira PJV, Pinheiro JL, Correia AA. Numerical analysis of an embankment built on soft soil reinforced with deep mixing columns: Parametric study. Comput Geotech 2011;38:566–76. http://dx.doi.org/10.1016/J.COMPGEO.2011.03.005.

[58] Pandey BK, Rajesh S, Chandra S. Time-dependent behavior of embankment resting on soft clay reinforced with encased stone columns. Transp Geotech 2022;36:100809. http://dx.doi.org/10.1016/J.TRGEO.2022.100809.

[59] Saltelli A, Ratto M, Andres T, Campolongo F, Cariboni J, Gatelli D, et al. Global sensitivity analysis: The primer. John Wiley & Sons; 2008.

[60] Czitrom V. One-factor-at-a-time versus designed experiments. Amer Statist 1999;53:126–31, URL: http://www.jstor.org/stable/2685731.

[61] Antony J. Design of experiments for engineers and scientists. 3rd ed.. chapter 1, Elsevier; 2023, p. 1–6. http://dx.doi.org/10.1016/C2022-0-01075-8.

[62] Campolongo F, Cariboni J, Saltelli A. An effective screening design for sensitivity analysis of large models. Environ Model Softw 2007;22:1509–18. http://dx.doi.org/10.1016/J.ENVSOFT.2006.10.004.

[63] Wu CFJ, Hamada M. Experiments: Planning, analysis, and optimization. In: Wiley series in probability and statistics. John Wiley & Sons, Inc.; 2021, http://dx.doi.org/10.1002/9781119470007.

[64] Montgomery DC. Design and analysis of experiments. 10 ed.. Hoboken, NJ: Wiley; 2020.

[65] Larsson S, Dahlström M, Nilsson B. A complementary field study on the uniformity of lime-cement columns for deep mixing. Proc Inst Civ Eng - Ground Improv 2005a;9(2):67–77. http://dx.doi.org/10.1680/grim.2005.9.2.67.

[66] Larsson S, Dahlström M, Nilsson B. Uniformity of lime-cement columns for deep mixing: A field study. Proc Inst Civ Eng - Ground Improv 2005b;9(1):1–15. http://dx.doi.org/10.1680/grim.2005.9.1.1.

[67] Larsson S, Stille H, Olsson L. On horizontal variability in lime-cement columns in deep mixing. Géotechnique 2005c;55(1):33–44. http://dx.doi.org/10.1680/geot.2005.55.1.33.

[68] Tahershamsi H, Dijkstra J. Using experimental design to assess rate-dependent numerical models. Soils Found 2021;62:101244. http://dx.doi.org/10.1016/J.SANDF.2022.101244.

[69] Bozkurt S, Abed A, Karstunen M. Alternative ways of modelling stabilised excavations. In: 19th nordic geotechnical meeting – Göteborg 2024. 2024, p. 1–12, URL:https://www.ngm2024.se/Papers/sinem_bozkurt_ngm2024.pdf.

[70] Cheng D, Reiner DM, Yang F, Cui C, Meng J, Shan Y, et al. Projecting future carbon emissions from cement production in developing countries. Nat Commun 2023;14:1–12. http://dx.doi.org/10.1038/s41467-023-43660-x.

[71] Sargent P, Hughes PN, Rouainia M. A new low carbon cementitious binder for stabilising weak ground conditions through deep soil mixing. Soils Found 2016;56:1021–34. http://dx.doi.org/10.1016/J.SANDF.2016.11.007.

[72] Hov S, Paniagua P, Sætre C, Rueslåtten H, Størdal I, Mengede M, et al. Lime-cement stabilisation of Trondheim clays and its impact on carbon dioxide emissions. Soils Found 2022;62:101162. http://dx.doi.org/10.1016/J.SANDF.2022.101162.

[73] Ramírez AL, Korkiala-Tanttu L. Stabilisation of malmi soft clay with traditional and low-CO2 binders. Transp Geotech 2023;38:100920. http://dx.doi.org/10.1016/J.TRGEO.2022.100920.

[74] Honjo Y. A probabilistic approach to evaluate shear strength of heterogeneous stabilized ground by deep mixing method. Soils Found 1982;22:23–38. http://dx.doi.org/10.3208/s{andf}1972.22.23.

[75] Porbaha A. State of the art in deep mixing technology. Part IV: Design considerations. Proc Inst Civ Eng - Ground Improv 2000;4:111–25. http://dx.doi.org/10.1680/grim.2000.4.3.111.

[76] Wong DYC, Sadasivan V, Isaksson J, Karlsson A, Dijkstra J. Trans-scale spatial variability of lime-cement mixed columns. Constr Build Mater 2024;417:135394. http://dx.doi.org/10.1016/j.conbuildmat.2024.135394.

[77] Åhnberg H. Consolidation stress effects on the strength of stabilised Swedish soils. Proc Inst Civ Eng - Ground Improv 2006;10:1–13. http://dx.doi.org/10.1680/grim.2006.10.1.1.

[78] Kitazume M, Terashi M. The deep mixing method. 1st ed.. CRC Press; 2013, http://dx.doi.org/10.1201/b13873.

[79] Axelsson M, Larsson S. Column penetration tests for lime-cement columns in deep mixing—Experiences in Sweden. In: Proceedings of the 2003 speciality conference on grouting at the third international conference on grouting and ground treatment, New Orleans, Louisiana. 2003, p. 681–94. http://dx.doi.org/10.1061/40663(2003)39.

[80] Paniagua P, Bache BK, Karlsrud K, Lund AK. Strength and stiffness of laboratory-mixed specimens of stabilised Norwegian clays. Proc Inst Civ Eng - Ground Improv 2022a;175:150–63. http://dx.doi.org/10.1680/jgrim.19.00051.

[81] Paniagua P, Falle FR, Hov S, Tekseth KR, Mirzaei F, Breiby DW. Comparing laboratory and field samples of lime–cement-improved Norwegian clay. Géotechnique Lett 2022b;12:265–71. http://dx.doi.org/10.1680/jgele.22.00067.

[82] Hov S, Larsson S. Strength and stiffness properties of laboratory-improved soft Swedish clays. Int J Geosynth Ground Eng 2023;9. http://dx.doi.org/10.1007/s40891-023-00432-3.

[83] Gunther J, Holm G, Westberg G, Eriksson H. Modified dry mixing (MDM) — A new possibility in deep mixing. In: Geotechnical engineering for transportation projects. American Society of Civil Engineers; 2004, p. 1375–84. http://dx.doi.org/10.1061/40744(154)127.

[84] Yu Y, Pu J, Ugai K. Study of mechanical properties of soil-cement mixture for a cutoff wall. Soils Found 1997;37:93–103. http://dx.doi.org/10.3208/sandf.37.4_93.

[85] Lee FH, Lee Y, Chew SH, Yong KY. Strength and modulus of marine clay-cement mixes. J Geotech Geoenvironmental Eng 2005;131:178–86. http://dx.doi.org/10.1061/(ASCE)1090-0241(2005)131:2(178).

[86] Puppala AJ, Bhadriraju V, Madhyannapu RS, Nazarian S, Williammee R. Small strain shear moduli of lime-cement treated expansive clays. Chapter, 2006, p. 58–70. http://dx.doi.org/10.1061/40870(216)5.

[87] Madhyannapu RS, Puppala AJ, Nazarian S, Yuan D. Quality assessment and quality control of deep soil mixing construction for stabilizing expansive subsoils. J Geotech Geoenvironmental Eng 2010;136:119–28. http://dx.doi.org/10.1061/(ASCE)GT.1943-5606.0000188.

[88] Yao K, Chen Q, Xiao H, Liu Y, Lee FH. Small-strain shear modulus of cement-treated marine clay. J Mater Civ Eng 2020;32:04020114. http://dx.doi.org/10.1061/(ASCE)MT.1943-5533.0003153.

[89] Larsson S. The nordic dry deep mixing method: Best practice and lessons learned. In: Proceedings of the deep mixing — An online conference. DFI Deep Foundation Institute; 2021, p. 30.